Current **A**pplied **S**cience and **T**echnology e-ISSN: 2586-9396

Curr. Appl. Sci. Technol. ….., Vol... (No...), e0269722

Research article

The Feasibility of Using Palm Oil Fuel Ash (POFA) as a Potential Proton Exchange Membrane for Microbial Fuel Cell Application in Comparison with Montmorillonite (MMT) Membrane

Thisha Abirami Sivasankar[1,2], Mohd Akmali Mokhter[1,2]*, Juhana Jaafar[2,3], Naoko Yoshida[4], Farhana Abdul Aziz[2,3] and Wan Norharyati Wan Salleh[2,3]

[1]Department of Chemistry, Faculty of Science, Universiti Teknologi Malaysia, 81310 UTM Johor Bahru, Johor, Malaysia
[2]Advanced Membrane Technology Research Centre (AMTEC), Universiti Teknologi Malaysia, 81310 Skudai, Johor Bahru, Malaysia
[3]Faculty of Chemical and Energy Engineering, Universiti Teknologi Malaysia, 81310 Skudai, Johor Bahru, Malaysia
[4]Institute of Materials and Systems for Sustainability, Department of Civil Engineering, Graduate School of Engineering, Nagoya University, Aichi 464-8603, Japan

Received: 3 November 2025, Revised: 5 January 2026, Accepted: 19 January 2026, Published: 10 April 2026

Abstract

The incorporation of waste-derived materials in membrane technology is gaining interest due to their low cost, favorable physical properties, and potential to improve membrane stability. These materials are also attractive for their renewability, low production energy, and environmental benefits. Therefore, this study investigates the use of palm oil fuel ash (POFA) as a proton exchange membrane (PEM) for microbial fuel cell (MFC) application, comparing with montmorillonite (MMT) membrane along with its antifouling properties. POFA and MMT membranes were prepared via a phase inversion method and were sintered at 1150°C. These membranes were hydrothermally coated with sodium dodecyl sulfate (SDS), producing POFA-SDS and MMT-SDS membranes. The POFA membranes exhibited higher conductivity (0.0926 mS/cm) and ion exchange capacity (0.913 meq/g) than the MMT (0.0079 mS/cm; 0.674 meq/g), while the MMT had a higher surface charge (−42.3 mV) than POFA (−17.6 mV). The MMT exhibited superhydrophilicity, while the POFA was moderately hydrophilic. With the attachment of SDS, the hydrophilicity of the POFA increased. Antifouling tests showed cell concentration reductions of 53.85% (POFA-SDS) and 66.27% (MMT-SDS), which were over two-fold higher than the pristine membranes. SEM-EDX revealed that the POFA-SDS had biofilm agglomeration with fewer attached microbes, suggesting better long-term antifouling potential. In MFC tests using municipal sewage as a feed, the pristine POFA and MMT showed low current densities (3.72 and 3.88 mA/m², respectively). SDS coating increased current density to 26.17 mA/m² for the POFA-SDS and 21.19 mA/m² for the MMT-SDS, with power densities of

*Corresponding author: E-mail: mohdakmali@utm.my
https://doi.org/10.55003/cast.2026.269722
Copyright © 2024 by King Mongkut's Institute of Technology Ladkrabang, Thailand. This is an open access article under the CC BY-NC-ND license (http://creativecommons.org/licenses/by-nc-nd/4.0/).

12.31 and 10.59 mW/m², respectively. Despite their relatively low baseline performance, the POFA demonstrated promising potential as sustainable proton exchange membrane (PEM) materials.

Keywords: Microbial fuel cell; palm oil fuel ash; waste derived; proton exchange membrane; antifouling; MMT

1. Introduction

Microbial fuel cell (MFC) is promising technology that can degrade wastewater and harvest energy synchronously. A bibliometric review on the general trend of MFC revealed that in 2001 there were only 3 research articles published on MFC related studies and after 2 decades in 2022 about 348 research articles published focusing on MFC, which indicated the rising research interest in the generation of clean energy without causing excess CO_2 emission (Bose et al., 2024). The need for MFC is high due to its parallel usage in power generation and wastewater treatment applications. MFC uses microbes to convert chemical energy into organic matter directly into electrical energy. Microbes present in wastewater break down organic matter, releasing electrons that flow through a circuit to generate electricity. While electrons travel to the cathode through the circuit, ions move through a membrane, where they react with oxygen to form water. This allows MFCs to produce power while simultaneously treating wastewater.

The key parameter in efficient MFC operation is the ion exchange membrane (Leong et al., 2013). An ion exchange membrane functions to selectively allow the passage of specific ions while maintaining the separation of different chambers in a system (Min & Logan, 2004). This selective ion transport helps facilitate essential processes such as electrical conductivity and chemical reactions. Additionally, by enabling controlled ion movement, the membrane plays a crucial role in maintaining pH balance across the chambers, ensuring stable and efficient operation (He et al., 2008). There are two types of ion exchange membrane used in MFC, which are Proton Exchange Membrane (PEM) and Anion Exchange Membrane (AEM). PEMs have negatively charged fixed groups and allow the selective passage of cations, repelling anions. AEMs on the other hand, contain positively charged fixed groups and act vice versa. Among these two membranes, PEMs have higher ionic conductivity, better durability, and more established commercial usage (Wang et al., 2022). The current PEMs used in MFCs (Nafion commonly) have several drawbacks including high cost, reliance on non-renewable materials, and limited viability for large-scale wastewater treatment (Hernández-Flores et al., 2019). They also suffer from biofouling issues, which lead to increased internal resistance and reduced performance. To address these issues, the use of ceramics was introduced to significantly enhance their mechanical stability and contribute to long-term operational stability while minimizing fouling. To further enhance the cost-effectiveness, ion transport and antifouling properties of ceramic membranes, low-cost materials such as clay-based montmorillonite (MMT) is widely used (Kedang et al., 2022; Verma et al., 2023).

MMT, characterized by its small particle size, is a natural clay mineral with higher negative charge density. This fixed negative charge of MMT occurs due to isomorphic substitution within its crystal structure (Wang et al., 2024). This characteristic of MMT gives it a unique advantage over other low-cost materials like ceramic oxides, mullite and earthenware. The negative charge of MMT attracts cations in the interlayer spaces and on external surfaces. These cations are quickly exchanged with other cations in the surrounding solution through ion exchange processes because they are weakly bonded.

MMT improves mechanical strength and ionic conductivity of membranes due to its high cation exchange capacity and swelling characteristics. Verma et al. (2023) indicated that membranes mixed with MMT increased MFC power output by 48% and improved ion exchange capacity by up to 1.6 times when compared to bare ceramic membranes. Incorporation of 3 wt.% MMT into Nafion® using methanol feed showed 20% efficiency in fuel cell test (compared to 13.72% for Nafion®117), while also raising the power density to 88 mW cm^{-2} (compared to 39 mW cm^{-2} for Nafion®117) (Hasani-Sadrabadi et al., 2010). In another study, 1:2 of chitosan and MMT blended PEM reached maximum power density of 229.12 mW/m², giving more than three times higher current, current density and columbic efficiency than membrane with chitosan alone (Yousefi et al., 2020). Hence, MMT-containing membranes are useful for MFC applications due to their improvements in proton transport and cation exchange capacity. These characteristics position MMTs as effective reference materials for evaluating the performance of waste derived membranes in lab scale studies aiming to reduce the membrane costs.

Currently, membranes for MFC are often expensive, synthetic, and environmentally unfriendly, with limited performance in treating complex wastewaters. This creates a need for alternative materials that are low-cost, sustainable, and functional. Waste-derived materials offer a promising solution, as they are eco-friendly, readily available, and can serve as high-performing membrane components by providing ion-conducting sites, surface functional groups, and acting as structural fillers or porosity modifiers (Al-Shaeli et al., 2022; Chakraborty et al., 2020). Utilization of waste materials for membrane development not only curtails the production and waste disposal costs but also promotes sustainability by providing value to the trash (Samadi et al., 2022). Bibliometric analysis from Scopus records from 2004-2024 indicates that research on membranes fabricated from waste materials has expanded sharply, with most of the growth occurring over the last five years (Sivasankar et al., 2025).

Waste derived materials have been widely used in modifying MFC electrodes due to their high electrical conductivity, porosity, and surface area. Anitha & Devi (2023) reviewed around 36 studies and highlighted that electrodes derived from waste materials including olive wood (Elleuch et al., 2015), waste coffee grounds (Jang et al., 2015), pistachio shells, pecan shells, saw dust (Konsolakis et al., 2015) and sunflower husks (Kacprzak et al., 2014) and many more were utilized to produce power densities up to 900 mWm^2 due to their remarkable conductivity in systems such as direct carbon fuel cells. In microbial fuel cells (MFCs), only a limited number of waste materials have been explored, primarily for electrode fabrication. Bamboo waste, coconut shell (Naveenkumar & Senthilkumar, 2021), and sewage (Yuan et al., 2013) have been used as electrodes, achieving power outputs of up to 500 mW/m². However, their potential use as membranes has been less investigated. For instance, sweet lime peel which was fabricated into a PEM membrane showed an ionic conductivity of 0.0204 S cm^{-1} with a maximum power density of 5.6 mW/m^2 (Bar et al., 2025). Mahino starch extracted from cassava root was integrated with clay material had a maximum proton transfer rate of 13.8 x 10^{-11}, 339 mV of maximum output voltage and with 50% COD removal of wastewater stimulated with yeast (Abdon et al., 2023). It is essential to note that these materials lowered the cost of production of the commonly used Nafion membranes by approximately 17 times (González-Pabón et al., 2019).

Palm oil fuel ash (POFA) is a waste material that is a byproduct from burning of palm kernel, mesocarp fiber and husk. Silicon dioxide is the major component of POFA and is followed by iron oxide and alumina, which are minor components. POFA surfaces are rich in oxides that can develop a negative charge similar to MMT. However, research studies into the electrochemical properties of POFA are scarce. Previously, POFA was

incorporated into hydrophobic polyvinylidene fluoride (PVDF) membrane, providing significant elevation in pure water flux from 40.16 to 81.08 L/m^2.h (Abuabdou et al., 2021). Moreover, the modification of POFA membranes with polyethersulfone (PES) as a binder significantly enhanced the removal of COD by up to 57.06%. The evaluation of hollow fiber POFA membranes revealed that they possessed the excellent mechanical strength of 98.1 MPa and high pure water flux of 123.2 L/m^2.h (Tai et al., 2021). In addition, Yusof et al. (2020a) revealed that POFA powder had maximum adsorption capacities of arsenic (As) of 95.62 and 98.34 mg·g^{-1} of As(III) and As(V), respectively. They treated POFA by calcination at 1150°C which successfully removed 48.7% and 50.2% of As(III) and As(V), respectively. In the same year, Yusof et al. (2020b) fabricated a POFA hollow fiber membrane using PES as a polymer binder, achieving adequate mechanical strength (52.84 MPa) and a high pure water flux of 250.73 L/m²·h. For further enhancement of POFA, the effect of pre-treated POFA was analyzed and it was depicted that the calcination at 700°C offered the highest oil rejection efficiency of 88.9% (Tai et al., 2019). From these studies, it is evident that the filtration and adsorption capacity of POFA are well established, but its ion exchange properties remain unexplored.

Hence, to address the limited exploration of POFA in ion exchange applications like MFCc, this study investigated the potential of POFA as a proton exchange membrane (PEM) for MFC applications. POFA and MMT were directly compared in this study with respect to their electrochemical and physicochemical characteristics for bioelectricity generation. By applying a coating of sodium dodecyl sulfate (SDS), this study was also aimed at improving their performance in MFC systems and evaluate their antifouling properties. This work advances the field by developing a low cost membrane for MFCs by demonstrating the potential of waste-derived PEMs. The baseline results of POFA-based PEMs in MFC applications can provide evidence in favour of their potential as an alternative to conventional membranes.

2. Materials and Methods

2.1 Materials

The materials used in this study included palm oil fuel ash (POFA, sourced locally in Palm oil mill, Kulai, Malaysia). The obtained POFA was dried, blended and sieved through a 200-mesh sieve and subsequently characterized using X-ray fluorescence (XRF) (Table 1). Montmorillonite clay (MMT-K30, Sigma-Aldrich, United States), N-methyl-2-pyrrolidone (NMP, ≥99.5% purity, Merck, Germany), polysulfone (PSF, Udel® P-3500, Solvay, Belgium), and Arlacel® (non-ionic surfactant additive, Croda International, United Kingdom) were used in this study. Milling was carried out using alumina jar (Nikkato Corporation, Japan). Deionized water was used as the non-solvent in the phase inversion process. Sodium dodecyl sulfate (SDS, ≥99% purity, Sigma-Aldrich, United States) was employed for membrane surface modification.

2.2 Fabrication of MMT and POFA flatsheet membranes

This study employed a phase inversion technique because it provides a controllable, versatile, cost-efficient way to fabricate membranes with tailored porous and asymmetric structures (Jung et al., 2016). To start, 40wt% by weight of POFA or MMT was dispersed into a solution containing NMP (solvent for dissolving PSF and dispersing POFA) and Arlacel (as an additive) inside a 500mL alumina jar. This suspension was then added with

one 20 mm and four 10 mm agate balls and were ball milled for 48 h. After 48 h of ball milling (NQM-2 planetary ball mill), the suspension was added with 10wt% PSF as a polymer binder and continued ball milling for another 2 days. After the completion of ball milling for a total 4 days, the suspension was degassed to remove air bubbles trapped into the suspension (Rasouli et al., 2019). The MMT and POFA suspensions in the alumina jars were then cast onto petri dishes to a thickness of 4 mm and underwent non-solvent induced phase separation. In this technique, the cast MMT and POFA suspensions were placed in a water bath where the NMP diffused out and water diffused in, triggering instantaneous phase separation. After immersing in the water bath for 24 h, the membranes were left to dry at room temperature and were sintered at 1150°C using Nabertherm Model LT 5/12 muffle furnace (Nawang et al., 2022). Sintering at 1150°C was essential to burn out PSF and remaining NMP, to densify the membrane particles into a mechanically robust network and to create interconnected ion channels. Sintering POFA membranes at this temperature matched MMT ceramic practices to give consistent densification, phase stability, and ionic conductivity (Silva et al., 2015). Figure 1 shows a schematic diagram of the method used to fabricate POFA and MMT membranes.

Table 1. Chemical oxide composition (wt.%) of sieved POFA determined by XRF

Chemical Composition	wt %
SiO_2	33.60
Al_2O_3	2.87
Fe_2O_3	33.80
MgO	13.60
CaO	6.66
K_2O	8.31
Others	1.16

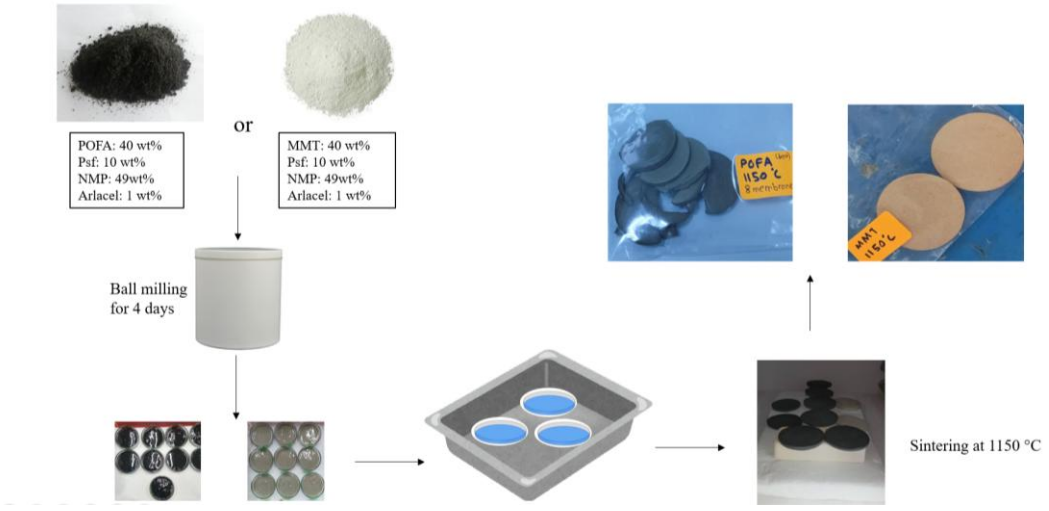


Figure 1. The schematic diagram of POFA and MMT membrane fabrication

2.3 Structural and physicochemical characterization

Upon fabrication, structural and physicochemical characterization of the POFA and MMT was evaluated. The crystallinity of both membranes was analyzed using XRD analytical technique. The basal spacing of the membranes was calculated via Bragg equation ($\lambda = 2d \sin \theta$). XRD measurements were performed using a SmartLab diffractometer (Rigaku, Japan) equipped with a Cu Kβ filter ($\lambda = 1.3922$ Å), operating at 40 kV and 30 mA. The functional groups present in each membrane were confirmed using Fourier Transform Infra-Red (FTIR) (PerkinElmer, United States). FTIR spectra were recorded using a PerkinElmer Spectrum One FTIR spectrometer over the range of 4000-400 cm^{-1} with a step size of 1 cm^{-1} in % transmittance mode. The water contact angle of the membranes was analyzed to determine the hydrophilicity of the MMT and POFA membranes. To measure the water contact angle, the dry membrane was placed flat on a goniometer. A 5 µL drop of water was dispensed onto the surface, and then a side-view image was immediately captured. Water uptake and porosity were calculated based on the weight and volume of the membrane as described in Nasr et al. (2022). Next, the three point bending test (Zwick/Roell Z020) was used to detect the mechanical strength of the membranes. Surface area was determined by the BET method (Micromeritics Tristar II, United States) and the pore volume and average pore diameter were obtained from the corresponding nitrogen adsorption–desorption isotherms (BJH analysis) using a gas sorption analyzer. The morphology of the POFA and MMT membranes was imaged using scanning electron microscopy (Hitachi model TM3000). Prior to imaging, each membrane surface was coated with a thin layer of gold by sputter coating.

2.4 Electrochemical and ion exchange analysis

The ion exchange capacity of the membranes was measured using the titration method. Initially, the dry MMT and POFA membranes were weighed and their mass recorded to establish a baseline for subsequent calculations. The membrane was then immersed in 30 mL of 2 M hydrochloric acid (HCl) for 24 h to protonate all ion exchange sites, ensuring complete conversion to the H^+ form. Following acid treatment, the membrane was transferred into 30 mL of 3 M sodium chloride (NaCl) solution for an additional 24 h to facilitate ion exchange, whereby Na^+ ions displaced H^+ ions from the membrane matrix into the solution. After removal, the resulting solution containing displaced H^+ ions were subjected to acid-base titration. A few drops of phenolphthalein indicator were added to the flask, and the solution was titrated with 0.01 M sodium hydroxide (NaOH) using a burette. The titration endpoint was determined when a light pink color appeared and stayed for at least 10 s, showing that all the H^+ ions had been neutralized. The volume of NaOH consumed was recorded, and the ion exchange capacity (IEC) (expressed in meq/g) was calculated using the formula:

$$\text{IEC} = \frac{\text{Concentration of NaOH} \times \text{Volume of NaOH}}{\text{Dry Membrane Weight}} \quad (1)$$

To measure the zeta potential, a Zetasizer (Malvern, United States) instrument was used. POFA and MMT membranes were mounted securely in the flow cell, ensuring there were no leaks. The cell was filled with a low-concentration electrolyte solution, such as 1 mM KCl, and air bubbles were removed. Measurements were taken in both flow directions and the values were averaged. This measurement uses deionized water as a

dispersant at a refractive index of 1.330 at 25°C. The built in conductivity probe measured the conductivity of the membrane with the aid of the electrolyte during the run.

2.5 Sodium dodecyl sulfate (SDS) coating

The prepared membranes were dissolved in 100mL of deionized water containing 20 g of SDS in a 500 mL hydrothermal autoclave vessel (Ramimoghadam et al., 2012). The vessel was then closed, fixed to the reactor and thermally heated in the oven at 120°C for 6 h. The method was repeated with a number of membranes, coating SDS onto the POFA and MMT membranes to produce POFA-SDS and MMT-SDS, respectively. After hydrothermal reaction, the membranes were left to dry at 40°C overnight. The interaction between POFA and MMT membranes with SDS can be observed in Figure 2a. In the presence of Na^+ ions, a cation-bridging mechanism occurs between SDS and the POFA/MMT membranes. The negatively charged functional groups on the membrane surface attract Na^+ ions, which partially neutralize the surface charge and act as electrostatic bridges between the membrane and the anionic head groups of SDS.

2.6 Antifouling properties evaluation

Two experiments were conducted to evaluate the antifouling properties of POFA, MMT, POFA-SDS and MMT-SDS membranes; (i) direct cell counting under fluorescence microscopy and (ii) surface characterization by scanning electron microscopy - energy dispersive x-ray spectroscopy (SEM-EDX) analysis. The POFA, MMT, POFA-SDS and MMT-SDS membranes were immersed in municipal sewage (Nagoya city, Japan) for 24 h and filtered. About 4.5 mL of phosphate-buffered saline with EDTA (PBSE) was first dispensed into an eppendorf tube, followed by the addition of 1 mL of the filtered sample. Each membrane after MFC operation, including MMT, MMT-SDS, POFA, POFA-SDS, and pure sewage, were then diluted 1000-fold. SYBERGREEN, a fluorescent nucleic acid stain, was added to the diluted samples, and the mixture was incubated in a dark area for 10 min to allow sufficient staining of the cells. After incubation, the samples were vacuum filtered to collect the stained cells onto a filter membrane. The filtered samples were then allowed to dry, and with the addition of a small amount of glycerol, each sample was visualized under a fluorescence microscope. The formation of biofilm on the surface of the membrane was further analyzed through SEM-EDX. Elemental mapping was conducted to identify the distribution of organic and inorganic foulants on the membrane surface.

2.7 MFC performance

A single chamber MFC setup consisted of a three-electrode configuration, where the working electrode (anode) was composed of carbon felt with platinum electrode, and the counter electrode (cathode) was made of activated carbon and carbon black cloth. The developed membrane was sandwiched between the anode and cathode carbon clothes. Figure 2b presents the schematic configuration and operating principle of the single-chamber MFC used in this study including the electrochemical reactions that occur within the system. At the anode, electroactive microorganisms oxidize biodegradable organic matter present in the sewage, generating electrons, protons (H^+), and carbon dioxide. The protons produced at the anode migrate through the PEM toward the cathode (Figure 2c). At the cathode, oxygen from the surrounding air acts as the terminal electron acceptor and reacts with the incoming electrons and protons to form water, completing the

electrochemical process. The anode chamber was filled with municipal sewage collected from Nagoya City, Japan as the substrate to support microbial activity. A reference electrode of Ag/AgCl was employed to accurately measure the anode potential. During operation, oxygen was supplied to the cathode chamber at a flow rate of 2 mL/min, while nitrogen gas was purged at 8 mL/min to maintain anaerobic conditions in the anode chamber. Electrochemical characterization was performed by recording open circuit voltage (OCV) and linear sweep voltammetry (LSV) curves. From these measurements, the anode potential was determined relative to the reference electrode, and the current density was calculated based on the electrode surface area and measured current, providing insights into the electrochemical performance of the MFC system. To calculate power density, Power density (P)=Current density (J) × Voltage (V) formula was used. This same system was replaced with remaining samples including POFA, MMT-SDS and POFA-SDS membranes.

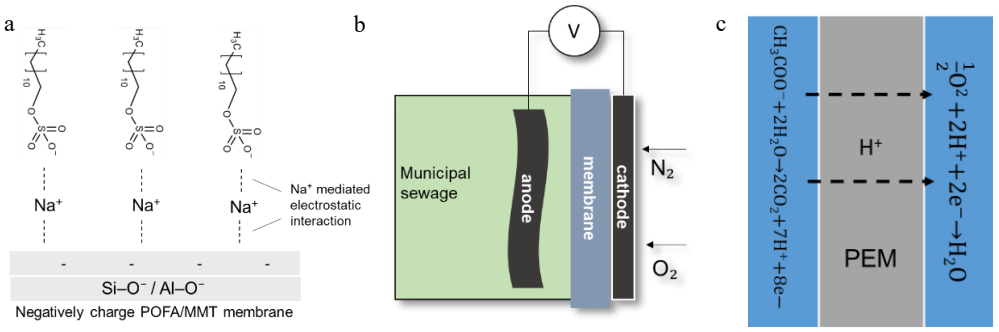


Figure 2. Schematic illustration of (a) Na^+-mediated electrostatic association of SDS on a negatively charged POFA/MMT membrane surface (b) Single-chamber MFC for municipal sewage treatment, illustrating the anode and air-cathode separated by a membrane (c) PEM associated with electrochemical reactions and proton transport mechanism.

3. Results and Discussion

3.1 Structural and physicochemical characteristics of MMT and POFA membranes

XRD was performed to analyze the crystallinity and d-spacing of the MMT and POFA membranes using Braggs law. A strong, sharp peak at 2θ = 10.62° refers to the basal reflection (001) of the MMT membrane demonstrates d-spacing of 0.8317 nm with good crystallinity. The higher-order basal reflections, such as 002 and 003, indicate well-ordered stacking of MMT layers. Higher angle peaks, including the Si–O peak near 25° and Al_2O_3-related peaks near 38°-40°, correspond to the tetrahedral and octahedral framework structure. Together, these reflections provide insight into both the layer ordering and structural integrity of MMT. This result is parallel with the layered structure of MMT, indicating the interlayer spacing between silicate sheets (Goonathilake & Bandaranayake, 2022). On the other hand, the POFA membrane shows broader peaks due to the presence of amorphous materials with some sharp peaks at 2θ = 20.83° and 26.64°, which are attributed to crystalline quartz (Tai et al., 2021). The POFA membrane also shows d-

spacings of 0.4263 nm (at 2θ = 20.83°) and 0.3343 nm (at 2θ = 26.64°) determined from the XRD pattern using Bragg's equation. The POFA results from XRD show partial crystalline, with a significant amorphous component. Garrote-Márquez et al. (2025) emphasized that the amorphous content enhances the membrane's ionic conductivity (). The XRD graph is illustrated in Figure 3.

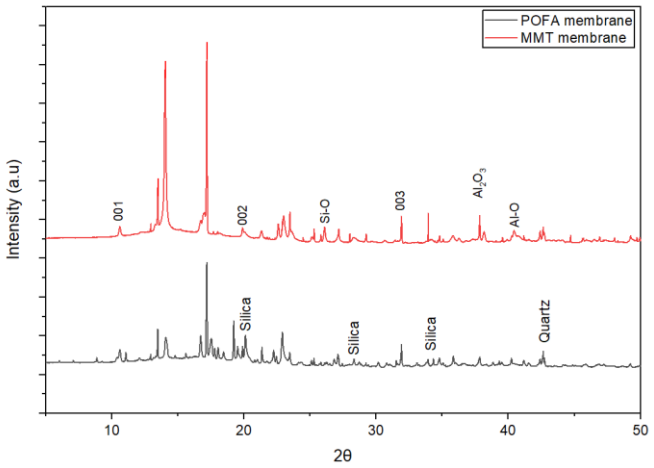


Figure 3. XRD results of POFA and MMT membranes

The functional groups of MMT and POFA membranes were confirmed by FTIR (Figure 4). A broad O–H stretching band centered at ~3400 cm^{-1} was observed in both membranes, indicating the presence of surface hydroxyl groups and physically adsorbed water molecules, which are essential for facilitating H^+ transport through hydrogen-bonded networks. The asymmetric stretching vibration of Si–O–Si in the 1100–1000 cm^{-1} region reflects the silicate framework present in both MMT and POFA membranes, corresponding to silicate-based materials such as quartz and amorphous silica. Similar Si–O–Si stretching bands were reported in previous POFA studies, confirming the dominance of silica phases in POFA powders (Mulizar, 2020; Opiso et al., 2023). In addition to these common features, the POFA membrane exhibits bands at ~800–780 cm^{-1} attributed to symmetric Si–O–Si stretching, as well as absorption in the 600–500 cm^{-1} region associated with metal–oxygen (M–O) vibrations arising from oxides of Fe, Al, Mg and Ca, which are typical constituents of POFA as displayed in Table 1. The presence of a bending vibration near ~1630 cm^{-1} further confirms the existence of adsorbed water on the POFA surface. For the MMT membrane, distinct bands at 3620–3650 cm^{-1} and ~880–915 cm^{-1} are assigned to Al–OH and Al–Mg–OH bending vibrations, respectively, indicating a dioctahedral MMT structure in which aluminum and magnesium cations occupy octahedral sites coordinated with hydroxyl ligands (Yaghmaeiyan et al., 2022). Additional lattice deformation bands observed below 600 cm^{-1} correspond to Si–O–Al and Si–O–Si vibrations, confirming the preservation of the layered aluminosilicate framework. Overall, the FTIR results demonstrate that while both membranes share hydroxyl groups and silicate networks, POFA possesses a more heterogeneous surface enriched with metal oxides, whereas MMT exhibits a well-ordered aluminosilicate structure with characteristic octahedral hydroxyl functionalities.

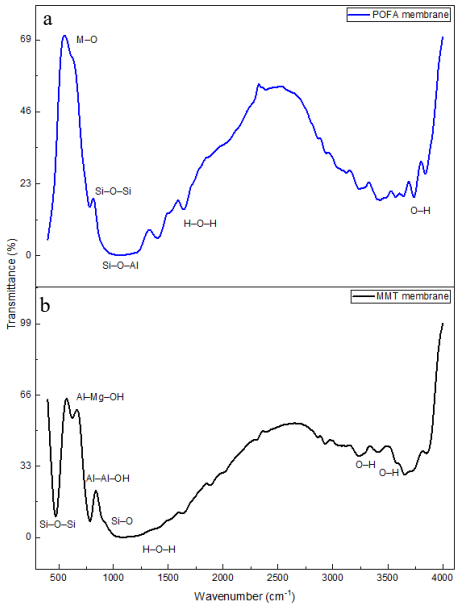


Figure 4. FTIR results of (a) POFA and (b) MMT membranes

The three point bending test was performed according to ASTM C674 standard. The average flexural strength obtained was 57.3 MPa for MMT, and 216.4 MPa for POFA membrane. Although there are few studies that report on the mechanical strength of bare MMT membranes, it is widely known that the incorporation of MMT with other materials in developing a composite membrane tremendously increases the flexural and tensile strength of the membrane (Gupta et al., 2021; Rahmatulloh et al., 2023). Generally, clay additives enhance membrane mechanical strength by reinforcing the polymer matrix, enabling effective stress transfer, and improving dimensional stability (Ahmad et al., 2026). A recent study on PSF/MMT mixed matrix membranes showed that increasing MMT loading can compromise mechanical integrity due to the hydrophilic nature of MMT. Meanwhile, POFA has demonstrated a flexural strength of 4 times better than MMT. High silica content generally exhibits high mechanical stability, in addition to that the amount of iron oxide in the POFA membrane of this study is considerably high (Table 1). The combination of silica and iron oxide as a major component, offer a good balance of fluxing agent, glassy phases with heighted mechanical stability (Montoya-Quesada et al., 2022).

The water absorption of a membrane is crucial for better ion transport. Typically, a contact angle less than 10° indicates superhydrophilicity. Due to the strong bonding between the surface molecules, superhydrophilic membranes easily absorb water. Since MMT membranes have hydroxyl groups that easily attract water, their water contact angle is generally low (Langsung, 2017). In this study, a stable contact angle was not formed due to immediate absorption of MMT membrane justifies its superhydrophilicity. This rapid uptake was supported by the Cobb test, which measured a high water absorption of 597 g/m², and was further facilitated by the membrane's high porosity (Figure 5e), allowing water to penetrate and fill the internal pore structure efficiently. However, the POFA membrane showed a moderate hydrophilicity of 54.4°, highlighting relatively strong adhesion forces between water molecule and the membrane surface. POFA particles generally exhibit no presence of hydroxyl group due to high temperature sintering, and

hence have reduced hydrophilic characteristics compared with MMT membranes. The low water uptake and porosity of the POFA membranes further confirm this behavior. However, after SDS modification, the hydrophilicity of POFA increased, as evidenced by a reduction in contact angle. While no measurable contact angle was observed for MMT–SDS, indicating that MMT retained its superhydrophilic character. The incorporation of SDS introduces highly polar sulfate head groups at the membrane surface, which promote strong hydrogen bonding with water molecules and enhance surface wettability (Parra et al., 2024). Consequently, the POFA–SDS membranes exhibited improved hydrophilicity relative to the pristine POFA, indicating by the reduced contact angle, as illustrated in Figure 5.

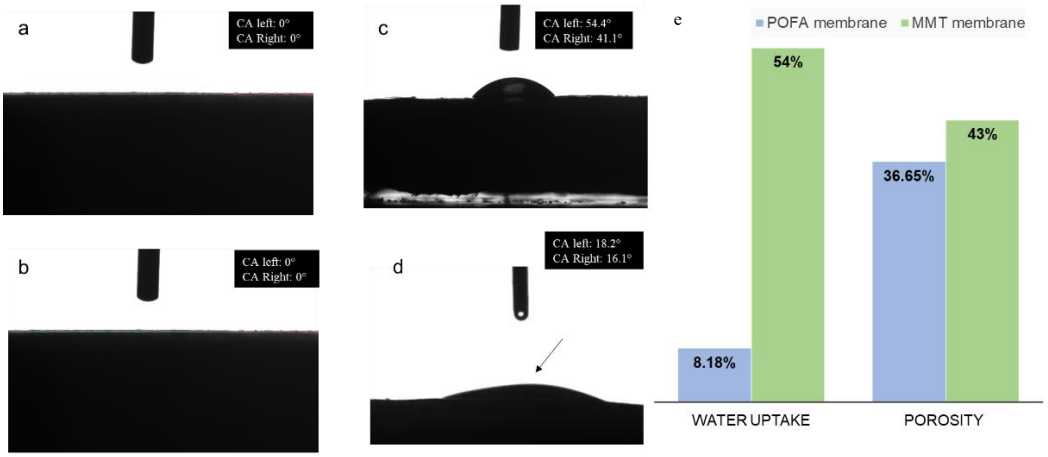


Figure 5. Water contact angle of (a) MMT, (b) MMT-SDS, (c) POFA and (d) POFA-SDS using sessile drop; (e) Graph of water uptake and porosity of MMT and POFA

Particle size analysis shows that that POFA has a higher pore volume and lower surface area than MMT membrane (Table 2). This is likely because POFA has coarser particle size, few large voids alongside many small, relatively closed pores which creates more void spaces for ion transport (Halim et al., 2025). As seen in SEM images (Figure 7), the large black “bubbles” and cavities may correspond to macropores formed from trapped air, ash agglomerates, or phase-inversion-induced voids linked to high pore volume in this study. A study on PVDF membranes incorporating silica based material as a filler reported that increasing silica content led to higher pore volume, which in turn enhanced ionic conductivity (Dyartanti et al., 2017). This supports the relationship observed in the present study, where increased pore volume facilitates more efficient ion transport across the membrane. In contrast, the MMT membrane has a much higher surface area in comparison to the POFA due of its nanoscaled and layered particles that provide abundant active sites for adsorption and diffusion. The MMT membranes exhibits wider mesopores, which promote efficient ion diffusion through larger, well-connected channels (Li et al., 2007), but its overall pore volume is smaller, indicating that these pores are fewer or thinner compared with the POFA membrane. Both MMT and POFA are classified within the mesoporous range (2-50 nm). Although the high surface area of MMT promotes ionic conductivity (Yang et al., 2019), the larger and more interconnected pore network of POFA facilitates more

efficient ion transport (García-Gabaldón et al., 2006), resulting in its higher overall conductivity and cation exchange capacity.

Additionally, both the POFA and MMT membranes exhibit Type IV nitrogen adsorption–desorption isotherms with clear hysteresis loops, consistent with their pore size falling within the mesoporous range of 2-50 nm (Figure 6). The more pronounced hysteresis loop observed for the MMT membrane indicates a more developed pore network. BJH pore size distribution analysis shows that the POFA membranes possesses a narrower distribution centered on smaller mesopores, whereas MMT exhibits a broader distribution shifted toward larger pore diameters, highlighting clear structural differences between the two membranes (Utama et al., 2018). According to Morishige (2021), the MMT membrane exhibits strong hysteresis and a broad pore size distribution, indicating significant pore blocking and interconnected pore network effects. In contrast, POFA shows weak hysteresis and a narrow pore size distribution, suggesting that pore blocking effects are minimal in this membrane.

Table 2. Particle size analysis of POFA and MMT membranes

Properties	POFA Membrane	MMT Membrane
Surface Area (m²/g)	0.23	0.48
Pore Volume (cm³/g)	0.00368	0.000257
Pore Size (nm)	5.77	12.95

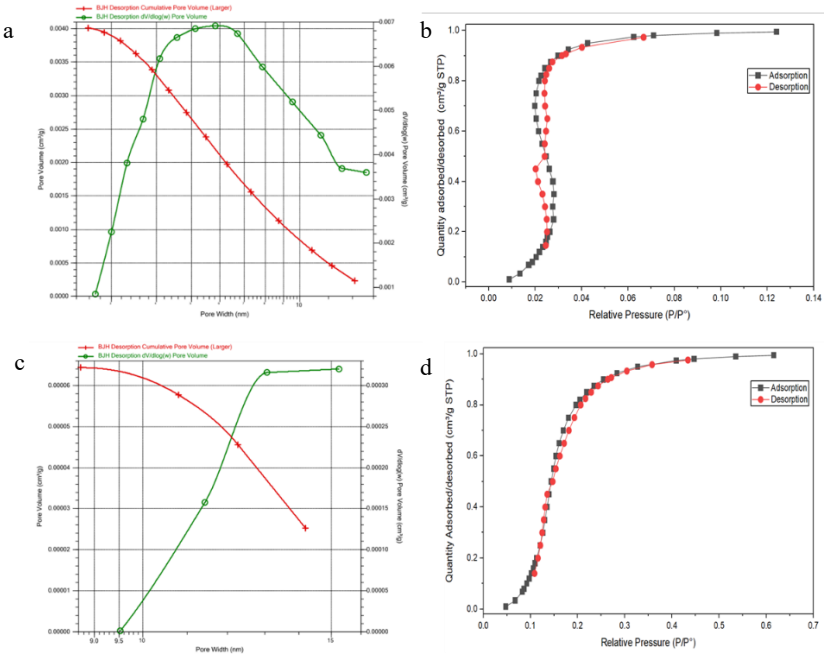


Figure 6. Nitrogen adsorption–desorption isotherms and BJH pore size distributions of the membranes: (a) nitrogen adsorption–desorption isotherm and (b) BJH pore size distribution of the POFA membrane; (c) nitrogen adsorption–desorption isotherm and (d) BJH pore size distribution of the MMT membrane

The surface morphology analysis reveals distinct differences between the MMT and POFA membranes that correlate well with their pore structure characteristics (Figure 7). The MMT membrane has a layered, plate-like structure with rough, uneven surfaces that have nodules and a porous network (Ching & Bak Lung, 2014). However, the POFA membrane exhibits a highly porous and heterogeneous morphology with loose particle packing, which accounts for the greater pore volume as shown in Table 2. SEM images of surface POFA reveal large black bubbles or holes, indicating regions that may not fully densify into a uniform matrix. These through-connected pores increase ion-transport pathways (Yusof et al., 2020b). Previous studies showed that such interconnected voids facilitate ionic conductivity by providing uninterrupted channels for hydrated ions, as larger pore networks reduce transport resistance (Wiedenmann et al., 2013). This structural feature helps to explain the comparable performance of POFA compared to the dense MMT membrane.

Earlier work on POFA hollow fiber membranes prepared with PESf shows that increasing sintering temperature drives grain growth and densification, causing thin pore walls to collapse. This process merges smaller pores into larger macropores, giving the structure an apparently more porous morphology, but with reduced effective surface area similar to POFA membrane in this study (Dyartanti et al., 2017). For MMT on the other hand, fine particle size and layered structure combine to create an enormous surface area. The visible nanoscale morphology confirms a high surface-area-to-volume ratio, which provides a large number of active sites necessary for strong ion exchange (Abulimiti et al., 2025). This finding is consistent with the porous structure of MMT observed in the SEM images and its inherently high surface area. Looking at the cross-sectional images of the POFA membrane, a relatively smooth surface punctuated by well-distributed spherical and irregular pores of varying sizes can be seen (Figure 7). These pores extend through the membrane thickness, forming interconnected and continuous void channels indicating a bulk porous network for ion transport. In comparison, the MMT membrane shows a more compact surface with densely packed, plate-like agglomerates displaying its limited macropore connectivity, dominated by stacked clay flakes and narrow interlayer spaces. Both MMT and POFA exhibit distinct morphologies, each playing a critical role in enhancing membrane performance for ion conductivity. Significant changes in the surface of these membranes can be observed upon hydrothermal coating as shown in Figure 8. Compared to pristine MMT, SDS-coated MMT shows granular deposits decorating the clay platelets, indicating SDS adsorption mainly along platelet edges via electrostatic interactions. In contrast, pristine POFA already has open pores and a smooth surface. After SDS modification, the SDS molecules coat the inside walls of the pores but do not block them. This coating makes the pores more hydrophilic because of the sulfate groups in SDS.

3.2 Electrochemical and ion exchange analysis

MMT is a prominent ceramic material with natural IEC due to its layered silicate structure. Due to the isomorphic substitution in MMT, some cations are replaced by others that have less positive charge producing permanent negative charge (Wang et al., 2024). To balance it, positive ions like Na^{+}, K^{+}, and Ca^{2+} move into the spaces between the layers and onto the surface and cause MMT to have cation exchange capacity. In this study, the IEC of the pristine MMT membrane is 0.674 meq/g whereas the IEC of the POFA membrane exhibits a notably higher IEC of 0.913 meq/g (Table 3). Although the IEC of POFA membranes has not been widely reported, POFA materials are well documented to exhibit high adsorption

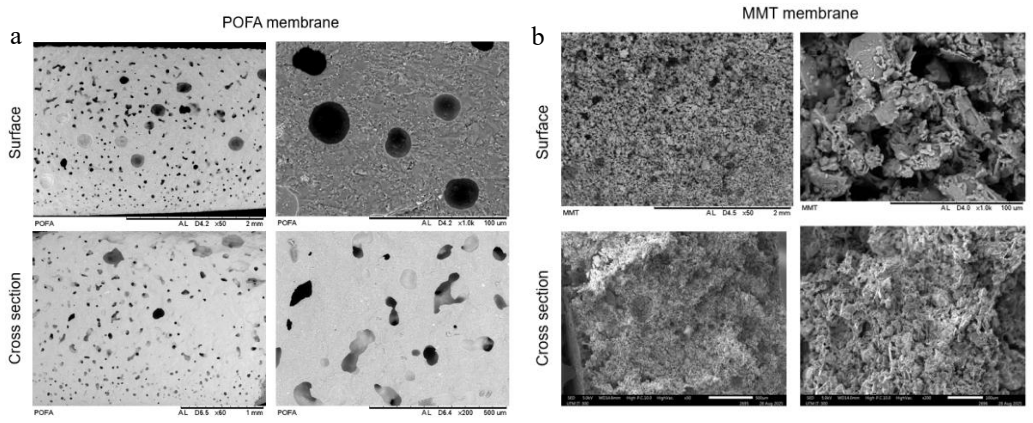


Figure 7. Surface and cross-sectional morphology of (a) POFA and (b) MMT membranes observed by SEM at different magnifications. Top row shows the surface and bottom row shows the cross-sectional morphologies

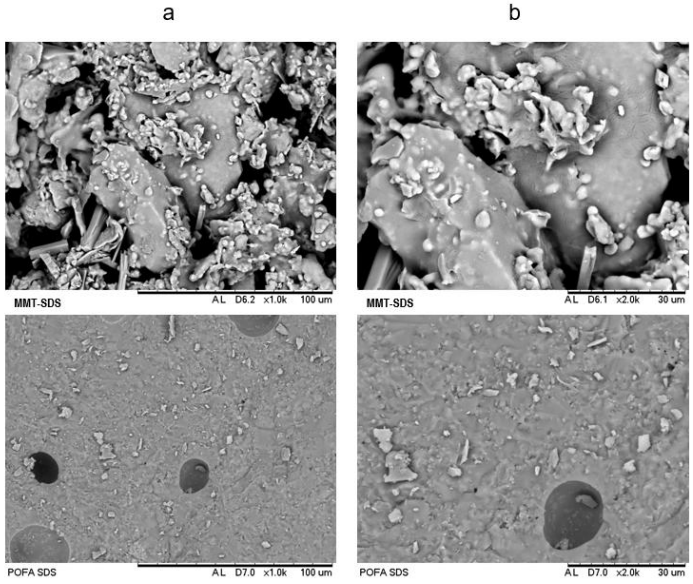


Figure 8. Surface morphology of (a) MMT–SDS and (b) POFA–SDS membranes at different magnifications

Table 3. Ion exchange capacity, surface charge and conductivity of MMT and POFA membrane

Membrane	Ion Exchange Capacity (meq/g)	Zeta Potential (mV)	Conductivity (mS/cm)
MMT	0.674	-42.3	0.0079
POFA	0.913	-17.6	0.0926

capacities toward heavy metals. Similar to POFA, fly ash and other waste-based membranes have reported elevated IEC values due to the dominance of chemically active adsorption sites rather than permanent lattice charge (Yusof et al., 2020a; Raji et al., 2023). This explains the relatively high IEC observed for the POFA membrane in the present study. Surface charge and conductivity measurements further support this interpretation. As expected, MMT exhibits a highly negative zeta potential due to isomorphic substitution within its layered aluminosilicate structure, which creates permanent negative charges and favors electrostatic ion exchange. However, such structural charge does not necessarily translate into high conductivity, as ion transport in MMT is largely confined to hydrated interlayer galleries and tortuous pathways, leading to limited charge mobility. Similar behavior was reported for other polymer membranes such as PSF, where the high surface charge exhibited poor ionic conductivity and high swelling ratio (Suhag et al., 2024). In contrast, the POFA membrane demonstrates significantly higher conductivity despite its lower net surface charge compared to the MMT membrane. High temperature sintering of POFA graphitizes residual biomass carbon into sp^2 domains, yielding delocalized π-electrons in the amorphous matrix that enable efficient electron shuttling (Abdallah et al., 2025). Thus, the high conductivity observed can be attributed to electrostatic interactions and calcination.

3.3 Antifouling properties

The number of microbes present in anolyte is imperative for efficient electron transfer. However, due to electrostatic force and the condition of membrane, microbes tend to be attached on the membrane and causing biofilm formation and membrane fouling (Pasternak et al., 2022). This situation degrades the membrane and hinders H^+ ion transport across the membrane, providing an unfavourable microbial environment and eventually causing biofouling. Direct cell counting reveals the microbial attachment, which is an early stage of biofilm formation. In this present study, high reduction percentage shows less microbial attachment and therefore, the ability of SDS coating to significantly reduce biofilm formation can be observed. The MMT-SDS and POFA-SDS membranes have the lowest cell concentrations (1.28×10^7 and 1.75×10^7 cells/mL) referring to their remarkable tendency to reduce microbial attachment. This means fewer cells are accumulating on these membranes compared to MMT and POFA without SDS modification. Figure 9 shows the results of direct cell counting through microbial attachment on membrane based on cell concentration and reduction percentage. The SEM-EDX results show the biofilm formation on MMT-SDS and POFA-SDS membranes surface (Figure 10). Relatively, POFA-SDS show the agglomeration of biofilm which is the non-attached bacterial aggregates, while MMT-SDS has attachment of bacteria in SEM-EDX (Li et al., 2013).

SDS is a widely used anionic surfactant that can significantly inhibit biofilm formation. SDS interferes with bacterial signalling pathways, altering the surface essential for adhesion (Sisay et al., 2023). SDS coatings on membranes typically reduce microbial attachment and biofilm formation by 70-95% in various applications (Fernández et al., 2007; Li et al., 2013; Zhang et al., 2025a). This prevents microbes from forming biofilm on membrane and significantly lowers the risk of biofouling. In this study, the SEM-EDX results justifies that POFA-SDS was better in reducing biofilm. This behavior can be attributed to the ability of POFA to promote SDS adsorption through hydrophobic interactions with its carbon-rich matrix and electrostatic attraction to its metal oxide components. As a result,

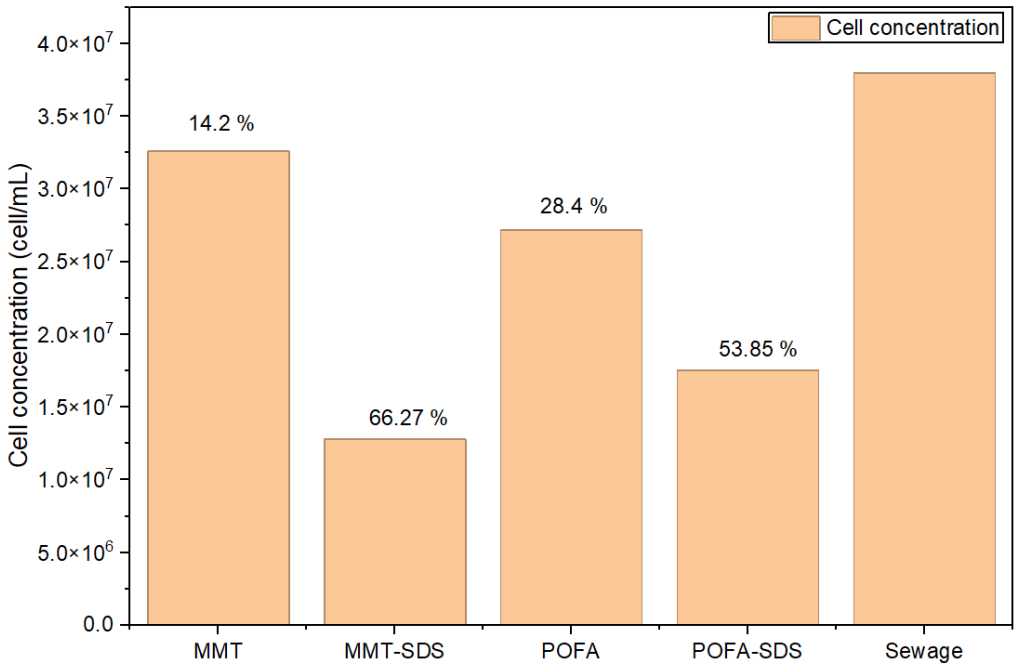
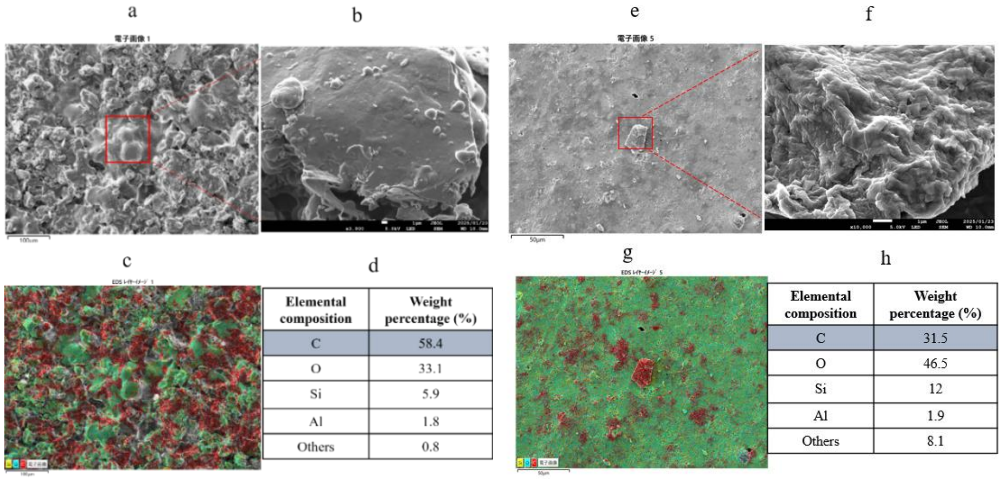


Figure 9. Microbial attachment on membrane based on cell concentration and reduction percentage



Elemental composition	Weight percentage (%)
C	58.4
O	33.1
Si	5.9
Al	1.8
Others	0.8

Elemental composition	Weight percentage (%)
C	31.5
O	46.5
Si	12
Al	1.9
Others	8.1

Figure 10. SEM-EDX images of MMT-SDS and POFA-SDS with elemental composition. SEM of MMT-SDS at (a) 500x magnification (b) 3000x magnification (c) EDX mapping (d) Elemental composition and weight percentage table based on EDX. SEM of POFA-SDS at (e) 500x magnification (f) 3000x magnification (g) EDX mapping (h) Elemental composition and weight percentage Table based on EDX

SDS molecules are more stably anchored onto the POFA surface. The outward orientation of the SDS alkyl chains leaves the sulfate head groups exposed, which enhances anti-biofilm. On the contrary, the limited edge-site cation exchange of MMT membrane enables weak SDS binding, hindered by repulsion from its negatively charged layers, reducing adsorption stability (Lin et al., 2011; Sun & Lei, 2023). Studies also shows that high surface area further promotes microbial attachment (Maitam et al., 2022; Zhang et al., 2025b) relevant to more bacterial attachment on MMT-SDS in Figure 10. Both MMT–SDS and POFA–SDS membranes effectively reduced microbial attachment compared to their pristine membranes, highlighting the functional role of SDS in limiting biofouling.

3.4 MFC performance

The utilization of POFA as a PEM provides a fundamental finding on the advantage of waste-derived membrane. Although both MMT and POFA show lower current densities of 3.88 and 3.72 mA/m^2, respectively, hydrothermal coating with SDS to introduce sulfate group enhances current generation by more than 6 times. The pristine POFA and MMT membranes demonstrate the ability to conduct electricity through ion exchange capacity (IEC), surface area, and pore volume. Since the POFA membrane is less hydrophilic than the MMT, the initial current density is slightly lower than the MMT membrane. The baseline current density of the bare MMT and POFA membranes provides sufficient fundamental current flow to enable operation of the MFC system. Figure 11 shows the anode polarization curve, which displays that the SDS modification of both POFA and MMT membranes dramatically enhances electrochemical activity captured by the current density value at the anode. Among them, POFA-SDS exhibits the maximum current density of 26.17 mA/m^2 while MMT-SDS shows 21.19 mA/m^2. The MMT-SDS membrane shows the most gradual slope suggesting better kinetic and lower resistance to electron transfer. Previous studies showed that the elevation of current density and power output upon SDS attachment enhanced electrocatalytic oxidation in methylene blue using titanium nanotubes (Xu et al., 2023). Yang et al. (2021) and Zhang et al. (2020) suggested that SDS modification allowed significant increase in surface area, providing more active sites for proton transport, and facilitating better charge transfer. As an example, the incorporation of SDS in the development of MOF–polyvinylpyrrolidone (PVP) electrodes successfully improved the coulombic efficiency to 96.1%. Zhong et al. (2022) attributed this enhancement to the presence of SDS, which facilitated the exposure of additional metal active sites within the MOF framework, thereby increasing electrochemical activity. This mechanism reasonably explains the nearly sixfold increase in current density upon SDS modification observed in the present study.

This study demonstrates a maximum power density of 12.31 mW m^{-2} for the POFA–SDS membrane, exceeding that of the MMT membrane and highlighting the potential of SDS-modified POFA as a PEM due to its enhanced performance. SDS modification increased the power density of both POFA and MMT membranes by approximately one order of magnitude, confirming the effectiveness of SDS as a cation-exchange additive for energy harvesting in MFC systems. Prior to SDS modification, both membranes exhibited comparable power densities, indicating similar baseline electrochemical performance. After SDS coating, POFA–SDS shows a more pronounced enhancement in power density and current density than MMT–SDS. This improvement is attributed to the open and interconnected pore structure of POFA, its higher pore volume, IEC, and conductivity, which collectively facilitate efficient ion transport. SDS introduces

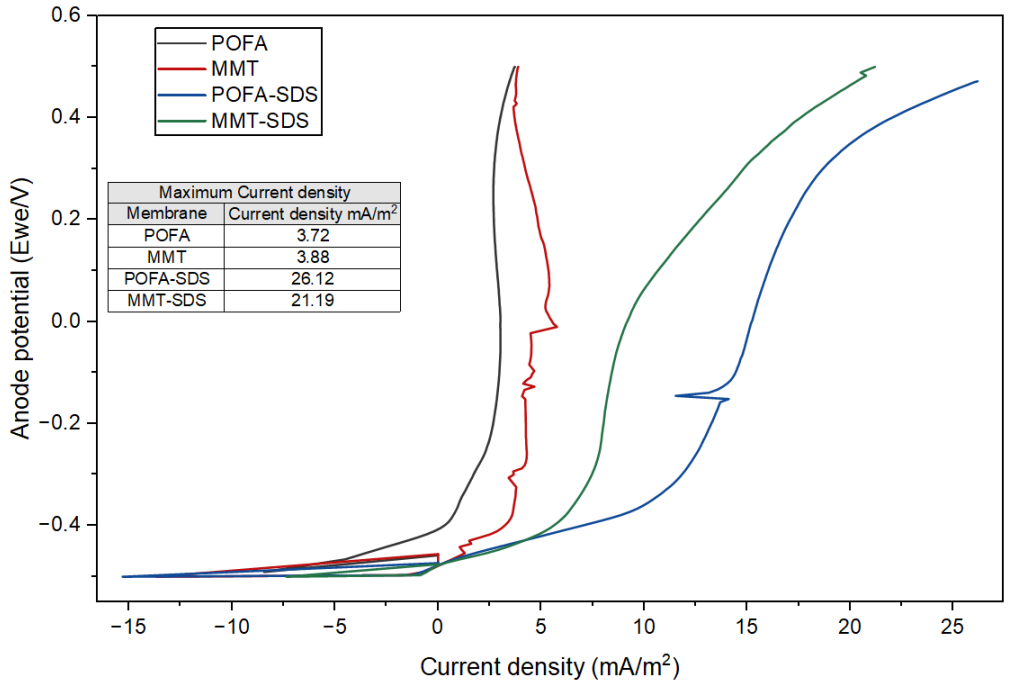


Figure 11. Polarization curve at anode potential against current density for MMT, MMT-SDS, POFA, POFA-SDS membranes

mobile counter-ions and polar sulfate groups, improving ion mobility, mitigating biofouling, and enhancing electrochemical performance (Liu et al., 2025). In contrast, although the MMT membrane possesses stronger intrinsic hydrophilicity and a more negative surface charge, ion transport in MMT is largely confined to flake-like mesopores with limited total pore volume, which can restrict effective ion migration under operating conditions. Moreover, the highly negative and strongly hydrophilic surface of MMT may limit stable SDS anchoring, reducing the contribution of SDS to ion transport and antifouling effects. This observation is consistent with previous reports showing that excessive hydrophilicity can increase cathodic resistance and adversely affect power density in MFC systems (Itoshiro et al., 2022). For POFA, SDS adsorption is promoted through a dual interaction mechanism. Electrostatic interactions occur between the anionic sulfate head groups of SDS and positively charged metal oxide sites on POFA, while hydrophobic interactions occurs between the alkyl chains of SDS and carbon-rich regions further stabilize SDS attachment (Liang et al., 2019). These synergistic interactions result in more ordered and stable SDS adsorption, leading to superior electrochemical performance compared to MMT–SDS. Based on LSV measurements, the resulting power densities are calculated and summarized in Table 4. Although the overall improvement is moderate, the superior power and current densities achieved by POFA-based membranes underscore their potential as viable PEMs for MFC applications.

Table 4. Comparison of power density generation of membranes of this study

Membrane	Power Density (mW/m²)
MMT	1.94
MMT-SDS	10.59
POFA	1.86
POFA-SDS	12.31

The feasibility of POFA as a PEM membrane is exceptionally evidenced in this study and provides a baseline finding for broader studies with POFA. To compare, mixtures of activated carbon from coconut shells, and Manihot starch- kaolin-clay was incorporated to produce a composite PEM, has a maximum output of 0.339 V (Abdon et al., 2023). Giant cane and terracotta-based PEM produced a very low maximum power output of 0.04 μW. while, using same waste material composite in anode electrode to elevated the conductivity achieving up to 40 mW/m^2 of power output (Cristiani et al., 2020). Sulfonated sweet lime peels were incorporated into a PVA-based membrane and employed as a PEM in a double-chamber MFC, achieving a notably high power density of 5.6 $mW\,cm^{-2}$ (Bar et al., 2025). While several studies have reported the potential use of waste materials in membrane development, most of them utilize waste as fillers, additives, or modify them prior to incorporation. Consequently, the electrochemical behavior of pristine waste remains poorly understood. Notably, primary PEMs from waste materials alone deliver power densities approaching those of benchmark MMT membranes, underscoring their practical efficacy.

4. Conclusions

The structural and functional advantages of POFA and MMT membranes highlighted their potential for PEM applications in MFC. The amorphous nature of POFA enables interconnected bond networks and efficient ion transport pathways, contributing to its superior mechanical stability, enhanced voltage performance, and a high IEC of 0.913 meq/g with a conductivity of 0.0926 S/cm. In contrast, the crystalline layered structure of MMT promoted enhanced water retention and surface activity. The POFA membranes also demonstrated a significantly higher flexural strength (216.4 MPa), approximately four times that of MMT, along with moderate hydrophilicity and lower crystallinity. SDS surface modification further enhanced both materials by improving anode potential by up to sixfold, boosting ion conductivity, and effectively reducing biofilm formation and microbial fouling. Notably, the POFA-SDS membranes exhibited more consistent performance, producing 26.12 mA/m^2 (current density) and 12.31 mW/m^2 (power density). In terms of mechanical stability, IEC, conductivity, maximum current density and antifouling properties, the POFA membrane outshined the performance of the MMT membrane. Current research has predominantly focused on the application of waste-derived materials in electrode development, leaving a knowledge gap regarding the performance of waste-derived membranes such as POFA or POFA–SDS. Given its low-cost, waste-derived origin and favorable electrochemical and mechanical properties, POFA emerges as a particularly promising material for durable, efficient, and sustainable MFC applications.

Despite the promising performance of POFA membranes as ion exchange membranes, several limitations remain that warrant further investigation. The moderate hydrophilicity of POFA, while beneficial for mechanical stability, may limit peak proton transport. Therefore, targeted surface functionalization is necessary to improve water uptake without inducing excessive swelling. While SDS modification improves biofouling resistance, it does not fully eliminate microbial colonization, suggesting that pairing SDS

with other antimicrobial agents could further extend membrane lifespan. Importantly, this study focused primarily on short-term performance, with limited insight into long-term operational stability, membrane fouling, and membrane degradation under continuous use. Critical factors such as cathode potential, oxygen crossover, pH gradients, ion transport dynamics, and substrate conversion efficiency were also insufficiently analyzed in this study. Future research should prioritize long-term studies under diverse wastewater conditions and explore hybrid membrane systems that combine mechanical robustness of POFA with the hydrophilicity of MMT to achieve balanced and scalable solutions for PEM-MFC applications.

5. Acknowledgements

The authors express their gratitude to the Ministry of Higher Education (MoHE) for the generous financial support provided under the Long-Term Research Grant Scheme (SATREPS 2023: 1.2) with grant vote number of R.J130000.7809.4L976 (SATREPS 2023: 1.2). This study was also supported by the Science and Technology Research Partnership for Sustainable Development (SATREPS), which is a collaborative effort between the Japan Science and Technology Agency (JST) and the Japan International Cooperation Agency (JICA).

6. Authors' Contributions

Thisha Abirami Sivasankar: performed the research and wrote the paper; Juhana Jafaar, Farhana Aziz and Wan Norharyati Wan Salleh: coordinated the research, contributed new reagents/analytic tools and project team member; Naoko Yoshida: designed research and contributed new reagents/analytic tools; Mohd Akmali Mokhter: analyzed the data.

ORCID

Thisha Abirami Sivasankar https://orcid.org/0000-0002-8395-383X
Mohd Akmali Mokhter https://orcid.org/0000-0002-0863-0678
Juhana Jaafar https://orcid.org/0000-0002-7245-8155
Naoko Yoshida https://orcid.org/0000-0003-1981-2829
Farhana Aziz https://orcid.org/0000-0003-4537-8421
Wan Norharyati Wan Salleh https://orcid.org/0000-0002-8212-3893

7. Conflicts of Interest

There is no conflict of interest to declare.

References

Abdallah, L., Gondran, C., Monnier, V., Vollaire, C., & Haddour, N. (2025). Influence of pyrolysis temperature on the properties and electrochemical performance of cedar wood-derived biochar for supercapacitor electrodes. *Bioengineering*, *12*(8), Article 841. https://doi.org/10.3390/bioengineering12080841

Abdon, R. G. P., Pelicano, X. J. B., Salundaga, L. J. M., & Viado, C. M. G. (2023). Performance study of double chamber microbial fuel cell operating with dihydrogen

phyllosilicate clay and activated carbon from coconut shells as proton exchange membrane. *Chemical Engineering Transactions*, *106*, 37-42.

Abuabdou, S. M. A., Bashir, M. J. K., Aun, N. C., Sethupathi, S., & Yong, W. L. (2021). Development of a novel polyvinylidene fluoride membrane integrated with palm oil fuel ash for stabilized landfill leachate treatment. *Journal of Cleaner Production*, *311*, Article 127677. https://doi.org/10.1016/j.jclepro.2021.127677

Abulimiti, M., Luo, J., Liu, J., Cheng, C., Guo, J., & Zhou, D. (2025). Exploring the environmental feasibility of montmorillonite integration in the electrochemical oxidation of acid mine drainage. *Separation and Purification Technology*, *375*, Article 133762. https://doi.org/10.1016/j.seppur.2025.133762

Ahmad, R., Ahmad, K., Shah, M. U. H., Khan, H., & Alhulaybi, Z. A. (2026). Mechanical enhancements in polymer and biopolymer nanocomposites. In *Polymer and biopolymer nanocomposites* (pp. 97-127). Woodhead Publishing. https://doi.org/10.1016/B978-0-443-26625-6.00012-7

Al-Shaeli, M., Al-Juboori, R. A., Al Aani, S., Ladewig, B. P., & Hilal, N. (2022). Natural and recycled materials for sustainable membrane modification: Recent trends and prospects. *Science of the Total Environment*, *838*(Part 1), Article 156014. https://doi.org/10.1016/j.scitotenv.2022.156014

Anitha, A., & Devi, N. R. (2023). Prospects of biochar as a renewable resource for electricity. In M. Bartoli, M. Giorcelli, & A. Tagliaferro (Eds.). *Biochar-productive technologies, properties and applications*. IntechOpen. https://doi.org/10.5772/intechopen.108161

Bar, A., Kupkar, O. J., Upadhyay, C., & Singh, R. (2025). Development of cost-effective proton exchange membrane using agro waste-based biochar for application in microbial fuel cell (MFC). *Biomass Conversion and Biorefinery*, *15*(6), 9205-9213.

Bose, D., Bhattacharya, R., & Mukherjee, A. (2024). Bibliometric analysis of research trends in microbial fuel cells for wastewater treatment. *Biochemical Engineering Journal*, *202*, Article 109155. https://doi.org/10.1016/j.bej.2023.109155

Chakraborty, I., Sathe, S. M., Dubey, B. K., & Ghangrekar, M. M. (2020). Waste-derived biochar: Applications and future perspective in microbial fuel cells. *Bioresource Technology*, *312*, Article 123587. https://doi.org/10.1016/j.biortech.2020.123587

Ching, O. P., & Bak Lung, M. W. (2014). Effects of montmorillonite (MMT) inorganic fillers on polyvinylidene (PVDF) mixed matrix membrane. *Applied Mechanics and Materials*, *625*, 696-700.

Cristiani, P., Goglio, A., Marzorati, S., Fest-Santini, S., & Schievano, A. (2020). Biochar-terracotta conductive composites: new design for bioelectrochemical systems. *Frontiers in Energy Research*, *8*, Article 581106. https://doi.org/10.3389/fenrg.2020.581106

Dyartanti, E. R., Susanto, H., Widiasa, I. N., & Purwanto, A. (2017). Response surface method (RSM) for optimization of ionic conductivity of membranes polymer electrolyte poly (vinylidene fluoride) (PVDF) with polyvinyl pyrrolidone (PVP) as pore forming agent. *IOP Conference Series: Materials Science and Engineering*, *206*, Article 012052. https://doi.org/10.1088/1757-899X/206/1/012052

Elleuch, A., Halouani, K., & Li, Y. (2015). Investigation of chemical and electrochemical reactions mechanisms in a direct carbon fuel cell using olive wood charcoal as sustainable fuel. *Journal of Power Sources*, *281*, 350-361.

Fernández, I. C. S., van der Mei, H. C., Lochhead, M. J., Grainger, D. W., & Busscher, H. J. (2007). The inhibition of the adhesion of clinically isolated bacterial strains on multi-component cross-linked poly (ethylene glycol)-based polymer coatings. *Biomaterials*, *28*(28), 4105-4112. https://doi.org/10.1016/j.biomaterials.2007.05.023

García-Gabaldón, M., Pérez-Herranz, V., Sánchez, E., & Mestre, S. (2006). Effect of porosity on the effective electrical conductivity of different ceramic membranes used

as separators in eletrochemical reactors. *Journal of Membrane Science*, *280*(1-2), 536-544.

Garrote-Márquez, A., Hernández, N. C., & Menéndez-Proupin, E. (2025). Correlation between C–H··· Br and N–H··· Br hydrogen bond formation in Perovskite CH3NH3PbBr3: A study based on statistical analysis. *Solids*, *6*(2), Article 29. https://doi.org/10.3390/solids6020029

González-Pabón, M. J., Figueredo, F., Martinez-Casillas, D. C., & Corton, E. (2019). Characterization of a new composite membrane for point of need paper-based micro-scale microbial fuel cell analytical devices. *PLoS One*, *14*(9), Article e0222538. https://doi.org/10.1371/journal.pone.0222538

Goonathilake, W. K. O. W., & Bandaranayake, P. W. S. K. (2022). Synthesis and characterization of lithium montmorillonite cathode material for Li-ion batteries. *Journal of Technology and Value Addition*, *4*(1), 37-51.

Gupta, G. K., Pandey, K., & Upadhyaya, P. (2021). Effect of montmorillonite clay content on the mechanical and thermal properties of flame retardant epoxy nanocomposites. *International Journal of Scientific Research in Mechanical and Materials Engineering*, *5*(1), 22-28.

Halim, N. I., Sidek, M. N. M., Newman, A., Saman, H. M., Suliman, N. H., & Fauzi, M. A. M. (2025). Nanomaterial-enhanced self-consolidating high-performance concrete: investigating the effects of nano POFA incorporation. *Journal of Mechanical Engineering*, *22*(1), 30-45.

Hasani-Sadrabadi, M. M., Dashtimoghadam, E., Majedi, F. S., Kabiri, K., Solati-Hashjin, M., & Moaddel, H. (2010). Novel nanocomposite proton exchange membranes based on Nafion® and AMPS-modified montmorillonite for fuel cell applications. *Journal of Membrane Science*, *365*(1-2), 286-293.

He, Z., Huang, Y., Manohar, A. K., & Mansfeld, F. (2008). Effect of electrolyte pH on the rate of the anodic and cathodic reactions in an air-cathode microbial fuel cell. *Bioelectrochemistry*, *74*(1), 78-82.

Hernández-Flores, G., Andrio, A., Compañ, V., Solorza-Feria, O., & Poggi-Varaldo, H. M. (2019). Synthesis and characterization of organic agar-based membranes for microbial fuel cells. *Journal of Power Sources*, *435*, Article 226772.

Itoshiro, R., Yoshida, N., Yagi, T., Kakihana, Y., & Higa, M. (2022). Effect of ion selectivity on current production in sewage microbial fuel cell separators. *Membranes*, *12*(2), Article 183. https://doi.org/10.3390/membranes12020183

Jang, H., Ocon, J. D., Lee, S., Lee, J. K., & Lee, J. (2015). Direct power generation from waste coffee grounds in a biomass fuel cell. *Journal of Power Sources*, *296*, 433-439.

Jung, J. T., Kim, J. F., Wang, H. H., Di Nicolo, E., Drioli, E., & Lee, Y. M. (2016). Understanding the non-solvent induced phase separation (NIPS) effect during the fabrication of microporous PVDF membranes via thermally induced phase separation (TIPS). *Journal of Membrane Science*, *514*, 250-263.

Kacprzak, A., Kobyłecki, R., Włodarczyk, R., & Bis, Z. (2014). The effect of fuel type on the performance of a direct carbon fuel cell with molten alkaline electrolyte. *Journal of Power Sources*, *255*, 179-186.

Kedang, Y. I., Priyangga, A., Atmaja, L., & Santoso, M. (2022). Characteristics and performance studies of a composite polymer electrolyte membrane based on chitosan/glycerol–sulfosuccinic acid modified montmorillonite clay. *RSC Advances*, *12*(47), 30742-30753.

Konsolakis, M., Kaklidis, N., Marnellos, G. E., Zaharaki, D., & Komnitsas, K. (2015). Assessment of biochar as feedstock in a direct carbon solid oxide fuel cell. *RSC Advances*, *5*(90), 73399-73409.

Langsung, A. M. (2017). Correlation between proton conductivity, hydrophilicity, and thermal stability of Chitosan/Montmorillonite composite membrane modified GPTMS and their performance in direct methanol fuel cell. *Malaysian Journal of Analytical Sciences*, *21*(3), 675-689.

Leong, J. X., Daud, W. R. W., Ghasemi, M., Liew, K. B., & Ismail, M. (2013). Ion exchange membranes as separators in microbial fuel cells for bioenergy conversion: a comprehensive review. *Renewable and Sustainable Energy Reviews*, *28*, 575-587.

Li, F., Wang, Z., Ergang, N. S., Fyfe, C. A., & Stein, A. (2007). Controlling the shape and alignment of mesopores by confinement in colloidal crystals: Designer pathways to silica monoliths with hierarchical porosity. *Langmuir*, *23*(7), 3996-4004.

Li, L., Molin, S., Yang, L., & Ndoni, S. (2013). Sodium dodecyl sulfate (SDS)-loaded nanoporous polymer as anti-biofilm surface coating material. *International Journal of Molecular Sciences*, *14*(2), 3050-3064.

Liang, Y., Guo, Y., Yang, X., Feng, R., Zhang, X., & Li, H. (2019). Insights on the interaction between sodium dodecyl sulfate and partially hydrolyzed microblock hydrophobically associating polyacrylamides in different polymer concentration regimes. *Colloids and Surfaces A: Physicochemical and Engineering Aspects*, *572*, 152-166.

Lin, K.-J., Jeng, U.-S., & Lin, K.-F. (2011). Adsorption and intercalation processes of ionic surfactants on montmorillonite associated with their ionic charge. *Materials Chemistry and Physics*, *131*(1-2), 120-126.

Liu, C., Gong, W., Iftikhar, T., Liu, W., Su, L., & Zhang, X. (2025). Iron-based metal-organic frameworks and their derivatives for high-performance supercapacitors. *Next Materials*, *7*, Article 100362. https://doi.org/10.1016/j.nxmate.2024.100362

Maitam, M. V. G., Nicolini, J. V., & de Araujo Kronemberger, F. (2022). Anti-fouling performance of polyamide microfiltration membrane modified with surfactants. *Journal of Applied Polymer Science*, *139*(42), Article e53015. https://doi.org/10.1002/app.53015

Min, B., & Logan, B. E. (2004). Continuous electricity generation from domestic wastewater and organic substrates in a flat plate microbial fuel cell. *Environmental Science and Technology*, *38*(21), 5809-5814.

Montoya-Quesada, E., Villaquirán-Caicedo, M. A., & de Gutiérrez, R. M. (2022). New glass-ceramic from ternary–quaternary mixtures based on Colombian industrial wastes: Blast furnace slag, cupper slag, fly ash and glass cullet. *Boletín de la Sociedad Española de Cerámica y Vidrio*, *61*(4), 284-299.

Morishige, K. (2021). Revisiting the nature of adsorption and desorption branches: Temperature dependence of adsorption hysteresis in ordered mesoporous silica. *ACS Omega*, *6*(24), 15964-15974. https://doi.org/10.1021/acsomega.1c01643

Mulizar, Fazliah, Iskandar, Aiyub, & Fauzi, A. (2020). Effect of POFA as a replacement material on fly ash based geopolymer mortar. *IOP Conference Series: Materials Science and Engineering*, *854*, Article 012012. https://doi.org/10.1088/1757-899X/854/1/012012

Nasr, M., Alfryyan, N., Ali, S. S., Abd El-Salam, H. M., & Shaban, M. (2022). Preparation, characterization, and performance of PES/GO woven mixed matrix nanocomposite forward osmosis membrane for water desalination. *RSC Advances*, *12*(39), 25654-25668.

Naveenkumar, M., & Senthilkumar, K. (2021). Microbial fuel cell for harvesting bio-energy from tannery effluent using metal mixed biochar electrodes. *Biomass and Bioenergy*, *149*, Article 106082. https://doi.org/10.1016/j.biombioe.2021.106082

Nawang, R., Hussein, M. Z., Matori, K. A., & Abdullah, C. A. C. (2022). Effect of sintering temperature on the specific surface area and compressive strength of hydroxyapatite/montmorillonite nanocomposite. *AIP Conference Proceedings*, *2506*(1), Article 030006. https://doi.org/10.1063/5.0083720

Opiso, E. M., Tabelin, C. B., Maestre, C. V., Aseniero, J. P. J., Arima, T., & Villacorte-Tabelin, M. (2023). Utilization of palm oil fuel ash (POFA) as an admixture for the synthesis of a gold mine tailings-based geopolymer composite. *Minerals*, *13*(2), Article 232. https://doi.org/10.3390/min13020232

Parra, J. G., Iza, P., Dominguez, H., Schott, E., & Zarate, X. (2024). Unveiling the hydrophilic nature of SDS surfactant through molecular simulations: Exploring the influence of charge distribution on interfacial properties in the vacuum/SDS/water system. *Journal of Molecular Liquids*, *401*, Article 124692. https://doi.org/10.1016/j.molliq.2024.124692

Pasternak, G., de Rosset, A., Tyszkiewicz, N., Widera, B., Greenman, J., & Ieropoulos, I. (2022). Prevention and removal of membrane and separator biofouling in bioelectrochemical systems: a comprehensive review. *IScience*, *25*(7). Article 104510. https://doi.org/10.1016/j.isci.2022.104510

Rahmatulloh, A., Hidayati, M. D., & Santosa, S. (2023). Preparation and permeability test of chitosan-montmorillonite modified polyvinyl alcohol composite membrane. *International Journal of Advanced Multidisciplinary Research and Studies*, *3*(4),683-686.

Raji, Z., Karim, A., Karam, A., & Khalloufi, S. (2023). Adsorption of heavy metals: mechanisms, kinetics, and applications of various adsorbents in wastewater remediation—a review. *Waste*, *1*(3), 775-805. https://doi.org/10.3390/waste1030046

Ramimoghadam, D., Hussein, M. Z. B., & Taufiq-Yap, Y. H. (2012). The effect of sodium dodecyl sulfate (SDS) and cetyltrimethylammonium bromide (CTAB) on the properties of ZnO synthesized by hydrothermal method. *International Journal of Molecular Sciences*, *13*(10), 13275-13293.

Rasouli, Y., Abbasi, M., & Hashemifard, S. A. (2019). Fabrication, characterization, fouling behavior and performance study of ceramic microfiltration membranes for oily wastewater treatment. *Journal of Asian Ceramic Societies*, *7*(4), 476-495.

Samadi, A., Gao, L., Kong, L., Orooji, Y., & Zhao, S. (2022). Waste-derived low-cost ceramic membranes for water treatment: Opportunities, challenges and future directions. *Resources, Conservation and Recycling*, *185*, Article 106497. https://doi.org/10.1016/j.resconrec.2022.106497

Silva, M. C. D., Lira, H. D. L., Lima, R. D. C. D. O., & Freitas, N. L. D. (2015). Effect of sintering temperature on membranes manufactured with clays for textile effluent treatment. *Advances in Materials Science and Engineering*, *2015*(1), Article 371697. https://doi.org/10.1155/2015/371697

Sisay, E. J., Al-Tayawi, A. N., László, Z., & Kertész, S. (2023). Recent advances in organic fouling control and mitigation strategies in membrane separation processes: a review. *Sustainability*, *15*(18), Article 13389. https://doi.org/10.3390/su151813389

Sivasankar, T. A., Mokhter, M. A., & Jaafar, J. (2025). A bibliometric and visual analysis on the utilization of waste materials for the development of membranes across various sectors: Insights from the scopus database. *Journal of Membrane Science and Research*, *11*(3), e730103. https://doi.org/10.22079/jmsr.2025.2052665.1704

Suhag, A., Goel, P., Eswaraswamy, B., & Chattopadhyay, S. (2024). Surface-modified nanoclay incorporated anion exchange membrane facilitating performance in self-humidifying bipolar membrane fuel cell. *International Journal of Hydrogen Energy*, *55*, 704-717.

Sun, Y., & Lei, A. (2023). Ca2+-facilitated adhesion of bacteria on the Na-montmorillonite surface. *ACS Omega*, *8*(3), 3385-3395.

Tai, Z. S., Hafiz Dzarfan Othman, M., Mustafa, A., Mohamed Dzahir, M. I. H., Hubadillah, S. K., Koo, K. N., Azali, M. A., Alias, N. H., Seng Ooi, B., & Kurniawan, T. A. (2021). Design and characterization of ceramic hollow fiber membrane derived from waste

ash using phase inversion-based extrusion/sintering technique for water filtration. *Journal of Asian Ceramic Societies*, *9*(1), 341-358.

Tai, Z. S., Hubadillah, S. K., Othman, M. H. D., Dzahir, M. I. H. M., Koo, K. N., Tendot, N. I. S. T. I., Ismail, A. F., Rahman, M. A., Jaafar, J., & Abd Aziz, M. H. (2019). Influence of pre-treatment temperature of palm oil fuel ash on the properties and performance of green ceramic hollow fiber membranes towards oil/water separation application. *Separation and Purification Technology*, *222*, 264-277.

Utama, P., Saputra, E., & Khairat. (2018). Effective utilizations of palm oil mill fly ash for synthetic amorphous silica and carbon zeolite composite synthesis. *IOP Conference Series: Materials Science and Engineering*, *345*, Article 012009. https://doi.org/10.1088/1757-899X/345/1/012009

Verma, P., Daverey, A., & Arunachalam, K. (2023). Development and characterization of novel low-cost engineered pine needle biochar and montmorillonite clay based proton exchange membrane for microbial fuel cell. *Journal of Water Process Engineering*, *53*, Article 103750. https://doi.org/10.1016/j.jwpe.2023.103750

Wang, J., Wang, B., Tongsh, C., Miao, T., Cheng, P., Wang, Z., Du, Q., & Jiao, K. (2022). Combining proton and anion exchange membrane fuel cells for enhancing the overall performance and self-humidification. *Chemical Engineering Journal*, *428*, Article 131969. https://doi.org/10.1016/j.cej.2021.131969

Wang, W., Wu, L., Chang, L., Yang, W., Si, L., Nan, H., Peng, W., & Cao, Y. (2024). Functionality developments in montmorillonite nanosheet: properties, preparation, and applications. *Chemical Engineering Journal*, *499*, Article 156186. https://doi.org/10.1016/j.cej.2024.156186

Wiedenmann, D., Keller, L., Holzer, L., Stojadinović, J., Münch, B., Suarez, L., Fumey, B., Hagendorfer, H., Brönnimann, R., & Modregger, P. (2013). Three-dimensional pore structure and ion conductivity of porous ceramic diaphragms. *AIChE Journal*, *59*(5), 1446-1457.

Xu, M., Gao, C., Zhang, X., Liang, X., Hu, Y., & Wang, F. (2023). Development of SDS-modified PbO2 anode material based on Ti3+ self-doping black TiO2NTs substrate as a conductive interlayer for enhanced electrocatalytic oxidation of methylene blue. *Molecules*, *28*(19), Article 6993. https://doi.org/10.1016/j.rechem.2022.100549

Yaghmaeiyan, N., Mirzaei, M., & Delghavi, R. (2022). Montmorillonite clay: Introduction and evaluation of its applications in different organic syntheses as catalyst: A review. *Results in Chemistry*, *4*, Article 100549. https://doi.org/10.1016/j.rechem.2022.100549

Yang, B., Qin, T., Bao, Z., Lu, W., Dong, J., Bin, D., & Lu, H. (2021). Synthesis of SDS-modified Pt/Ti3C2Tx nanocomposite catalysts and electrochemical performance for ethanol oxidation. *Nanomaterials*, *11*(12), Article 3174. https://doi.org/10.3390/nano11123174

Yang, Y., Narayanan Nair, A. K., & Sun, S. (2019). Layer charge effects on adsorption and diffusion of water and ions in interlayers and on external surfaces of montmorillonite. *ACS Earth and Space Chemistry*, *3*(11), 2635-2645.

Yousefi, V., Mohebbi-Kalhori, D., & Samimi, A. (2020). Start-up investigation of the self-assembled chitosan/montmorillonite nanocomposite over the ceramic support as a low-cost membrane for microbial fuel cell application. *International Journal of Hydrogen Energy*, *45*(7), 4804-4820.

Yuan, Y., Yuan, T., Wang, D., Tang, J., & Zhou, S. (2013). Sewage sludge biochar as an efficient catalyst for oxygen reduction reaction in an microbial fuel cell. *Bioresource Technology*, *144*, 115-120.

Yusof, M. S. M., Othman, M. H. D., Wahab, R. A., Jumbri, K., Razak, F. I. A., Kurniawan, T. A., Samah, R. A., Mustafa, A., Rahman, M. A., Jaafar, J., & Ismail, A. F. (2020a). Arsenic

adsorption mechanism on palm oil fuel ash (POFA) powder suspension. *Journal of Hazardous materials*, *383*, Article 121214. https://doi.org/10.1016/j.jhazmat.2019.121214

Yusof, M. S. M., Othman, M. H. D., Wahab, R. A., Samah, R. A., Kurniawan, T. A., Mustafa, A., Rahman, M. A., Jaafar, J., & Ismail, A. F. (2020b). Effects of pre and post-ozonation on POFA hollow fibre ceramic adsorptive membrane for arsenic removal in water. *Journal of the Taiwan Institute of Chemical Engineers*, *110*, 100-111.

Zhang, J., Bo, S., Wang, C., Jian, Z., Chu, Y., Qiu, S., Chen, H., Xiong, Q., Yang, X., Xiao, Z., & Liu, G. (2025a). Fouling mitigation of PVDF membrane induced by sodium dodecyl sulfate (SDS)-TiO_2 micelles. *Membranes*, *15*(11), Article 330. https://doi.org/10.3390/membranes15110330

Zhang, K., Hu, H., Li, S., He, Y., & Guo, J. (2020). Effect of sodium dodecyl sulfate (SDS) on mechanical performance of polyvinyl-acetate-based emulsion polymer isocyanate. *International Journal of Adhesion and Adhesives*, *98*, Article 102539. https://doi.org/10.1016/j.ijadhadh.2019.102539

Zhang, T., Wang, W., Zhi, X., Ye, X., Wang, R., Zhao, J., Dai, J., Qiang, H., Liu, P., & Jia, H. (2025b). Substrate type-driven differences in interfacial microbial community and pathogenic risk: Clay, microplastics and activated carbon. *Gondwana Research*, *143*, 157-165. https://doi.org/10.1016/j.gr.2025.03.017

Zhong, N., Wu, W., Xu, F., Sun, L., Wu, Y., Lao, J., Qin, X., Wang, Y., Ding, X., Peng, A., Liu, J., & Yuan, D. (2022). Effect of SDS and PVP surfactants on synthesis of a flower-shaped porous Ni-MOFBDC@ C as electrode materials for high performance supercapacitor. *International Journal of Electrochemical Science*, *17*(5), Article 220540. https://doi.org/10.20964/2022.05.34